HHS Public Access

Author manuscript

J Phys Chem B. Author manuscript; available in PMC 2017 July 02.

Published in final edited form as:

J Phys Chem B. 2017 March 02; 121(8): 1749–1757. doi:10.1021/acs.jpcb.6b06822.

Wavelength-Dependent Second Harmonic Generation Circular Dichroism for Differentiation of Col I and Col III Isoforms in Stromal Models of Ovarian Cancer Based on Intrinsic Chirality Differences

Kirby R. Campbell and **Paul J. Campagnola***

Department of Biomedical Engineering, University of Wisconsin-Madison, 1550 Engineering Drive, Madison, Wisconsin 53706, United States

Abstract

Extensive remodeling of the extracellular matrix (ECM) occurs in many epithelial cancers. For example, in ovarian cancer, upregulation of collagen isoform type III has been linked to invasive forms of the disease, and this change may be a potential biomarker. To examine this possibility, we implemented wavelength-dependent second harmonic generation circular dichroism (SHG-CD) imaging microscopy to quantitatively determine changes in chirality in ECM models comprised of different Col I/Col III composition. In these models, Col III was varied between 0 and 40%, and we found increasing Col III results in reduced net chirality, consistent with structural biology studies of Col I and III in tissues where the isoforms comingle in the same fibrils. We further examined the wavelength dependence of the SHG-CD to both optimize the response and gain insight into the underlying mechanism. We found using shorter SHG excitation wavelengths resulted in increased SHG-CD sensitivity, where this is consistent with the electric-dipole-coupled oscillator model suggested previously for the nonlinear chirality response from thin films. Moreover, the sensitivity is further consistent with the wavelength dependency of SHG intensity fit to a two-state model of the two-photon absorption in collagen. We also provide experimental calibration protocols to implement the SHG-CD modality on a laser scanning microscope. We last suggest that the technique has broad applicability in probing a wide range of diseased states with changes in collagen molecular structure.

Graphical Abstract

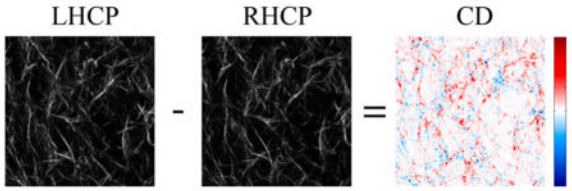

*Corresponding Author: pcampagnola@wisc.edu.

ORCID

Paul J. Campagnola: 0000-0002-2870-7249

Notes

The authors declare no competing financial interest.

1. INTRODUCTION

Dynamic remodeling of collagen composition and structure has been observed to be a critical step in the initiation and progression of many epithelial cancers.[1,2] For example, in ovarian cancer, this is manifested in the increase (and/or reorganization) of collagen types I, III, and VI (Col I, III, and VI) as well as other structural and compositional alterations in the extracellular matrix (ECM).[1,3] These collagen isoforms are composed of different individual α-chains, suggesting their incorporation into fibrillar networks might be detectable by structural-based analyses. Successful detection of relative concentrations in tissue may assist in elucidating risk of onset and/or progression of ovarian cancer risk. Previous studies have primarily utilized immunofluorescent microscopy and Western blots for examining their distribution in ovarian (and other) tissues, but these techniques lack specificity between isoforms (especially for Col I and Col III which have similar epitopes) and are often not quantitative.[4,5]

Second harmonic generation (SHG) microscopy, in contrast, directly visualizes fibrillar collagen with high specificity and sensitivity without the need of exogenous labels. In the past decade, SHG imaging has shown great promise for detecting the associated ECM remodeling in many diseases, including cancers, fibroses, artherosclerosis, osteoarthitis, and connective tissue disorders.[6–16] Due to the underlying photophysics, SHG microscopy provides subresolution details (macro- and supra-molecular) of collagen via unique responses based on fibrillar composition and/or assembly.[16–20] Polarization-resolved SHG analyses are particularly powerful, as they can be related to underlying collagen molecular properties. For example, in the single-axis molecular model, we showed that the SHG intensity response as a function of polarization excitation can be related to the pitch angle of the collagen α-helix.[21] Additionally, Barzda and co-workers have used polarization in/polarization out analyses to relate tensor matrix elements to specific components of the collagen molecule.[22]

We recently developed a pixel-based SHG polarization analysis that combined the single-axis model with the generic model by Brasselet.[23] This approach successfully delineated Col I from Col III in fibrillar gel models for ovarian cancer based on differences in the α-pitch angle of the two isoforms.[24] Here, we now implement wavelength-dependent SHG combined with circular dichroism (SHG-CD) as a complementary polarization scheme to further probe the structure in these in vitro models, where this approach is sensitive to the overall chirality of the collagen structural assembly. Conventional CD examines protein folding by measuring absorption differences of left-and right-handed (LH and RH) circularly polarized (CP) excitation, where this is reflective of the intrinsic protein chirality of the secondary and/or tertiary structure. While related, SHG-CD is not completely analogous to conventional CD due to the coherence and nonlinearity of the former. In landmark work, Hicks and co-workers showed 100% modulation of the resonance-enhanced SHG-CD from a film of chiral molecules with right-handed and left-handed circular polarized light,[25] where this was ascribed to coupling of chirality into the second-order response. Later, Verbiest et al. suggested that enhanced SHG could result from supra-molecular chirality, where they observed this in ordered helicenes and showed that higher order structures governed the observed response.[26]

We previously implemented the SHG-CD approach into laser scanning microsopy to examine change of structure in collagenous tissues. We found quantitative differences in human skin from normal patients versus those with the diseased state osteogenesis imperfecta, which results from misfolded collagen.[27] This work demonstrated for the first time the viability of the method in examining tissue structures with SHG-CD contrast, and this has now been reported for other tissues.[28]

We now address three issues to better establish the SHG-CD method for both basic science and translational approaches: (i) Optimize the instrumentation for accuracy. While the SHG-CD in skin and tendon tissues is much larger than the ~0.1% of ordinary CD (which also requires a melting curve), the response is ~20–45% and requires careful calibration to achieve accurate measurements. (ii) Optimize the wavelength to achieve sensitivity and better understand the contrast mechanism in tissues. This is important, as the underlying contrast of SHG-CD, i.e., the coupled oscillator (Kuhn model) or single electron model (Kauzmann model),[29] is not fully understood even on chiral surfaces and has not been explored in tissues. For example, a better understanding of the operative electric and magnetic interactions would provide insight into optimizing sensitivity and nonlinear chirality of materials in general. (iii) Then, apply the method to stromal models of ovarian cancer of differing Col I and III composition. We expect a differential response in net chirality manifested in the SHG-CD response with different balances of Col I and III composition as the α-chain incorporation in each isoform is different ($2\alpha_1\alpha_2$ and $3\alpha_1$, respectively).

This approach could lead to a new diagnostic approach for ovarian cancer, other cancers, and other diseased states where there are changes in collagen isoform distribution.[30,31]

2. MATERIALS AND METHODS

2.1. Sample Preparations

a. Preparation of Self-Assembled Collagen Gels—Self-assembled collagen gels were polymerized as previously described by Keely et al.[32] Briefly, type-I rat-tail collagen (BD Biosciences, Frankline Lakes, NJ) and recombinant human type-III collagen (Cell Sciences, Canton, MA) were neutralized with an equal volume of 100 mM HEPES in 5× phosphate-buffered saline (PBS) to obtain 1 mL gel volumes (~100 μm in thickness). The total collagen concentration equaled 2 mg/mL, but relative isoform concentrations were varied to achieve 100:0, 95:5, 90:10, 85:15, 80:20, and 60:40% Col I/Col III gels. Higher concentrations of Col III did not form stable gels. We allowed the collagen gels to polymerize at 37 °C for 5 h, and then, they were subsequently fixed in 4% paraformaldehyde and washed with PBS. Three gel replicates were analyzed separately, as the degree of polymerization can vary between collagen syntheses. To allow for self-consistent comparison between gels of varying concentrations of Col III, all collagen gels within a single experimental run were synthesized at the same time in two six-well plates allowing for duplicates of each gel each to be imaged at five distinct locations.

b. Preparation of Vesicles for Calibration—Giant unilamellar vesicles (GUVs) were created from L-a-phosphatidylcholine lipid (Avanti Polar Lipids; Alabaster, AL) for circular

polarization calibration. These are prepared by first dissolving the lipid in ethanol/chloroform, then drying with argon, and then slowly rehydrating in water.[33] The vesicles were stained with the membrane dye Di-8-ANEPPS (Invitrogen, Carlsbad, CA) at 10 μM concentration.

2.2. Experimental Microscope Setup

The SHG experimental imaging system with CD modifications was described in detail by Lien et al.[34] A laser scanning unit (FluoView 300; Olympus, Melville, NY) was mounted on an upright microscope (BX61; Olympus) and coupled to a mode-locked titanium sapphire laser excitation source with a pulse width and repetition rate of ~100 fs and ~80 MHz, respectively (Mira; Coherent; Santa Clara, CA). All imaging was performed with an average power controlled by an electro-optic modulator (ConOptics; Danbury, CT) of 15–40 mW at the focal plane using a 40× 0.8 NA water immersion lens (LUMPlanFL; Olympus) and a 0.9 NA condenser below the sample for forward photon collection. Forward SHG was detected by a photon counting photomultiplier module (7421 GaAsP Hamamatsu, Japan), where the SHG emission wavelengths of 390, 415, and 445 nm were first isolated using 10 nm wide bandpass filters (Semrock; Rochester, NY). The excitation wavelength was validated using a fiber-optic spectrometer (Ocean Optics; Dunedin, FL). The 512 × 512 pixel image field of view size was 85 × 85 μm^2, and the scanning speed was 2.71 s/frame with a three-frame Kalman average.

A liquid crystal modulator (LCM; LPR-200-850; Meadow-lark Optics, Frederick, CO) was mounted in the infinity space of the BX61 microscope with a subsequent quarter-wave plate. This configuration allows rapid (10^{-3} s) motion free rotation of the input linear polarization by 90° to provide switching between LHCP and RHCP states at the focus. No polarization analysis of the signal was performed. A custom LABVIEW program (National Instruments; Austin, TX) controlled the electro-optic modulator and LCM using a data acquisition card (PCI-6024E; National Instruments).

2.3. SHG-CD Calibration

As the normalized SHG-CD response is ~20–45%, it is critical to ensure that true left- and right-circular polarization, with minimal ellipticity, is achieved at the microscope focus to obtain accurate measurements. The LCM was initially set and calibrated to achieve optimal LHCP and RHCP orientation for the 890 nm excitation wavelength. Due to the wavelength dependence of the birefringence of the liquid crystal and other elements in the beam path, a Soleil-Babinet Compensator (Coherent Optics, Santa Clara, CA) was implemented before the microscope to precisely adjust the zero-order retardance for the shorter excitation wavelengths. For this assessment of the excitation polarization near the focal plane, the objective was temporarily removed and a Glan-Laser Polarizer (GLP; ThorLabs; Newton, NJ) followed by a power meter (Newport, Mountainview, CA) that was mounted in its stead. We use this hardware for power throughput measurements of various orientations of the GLP for use in the Stokes vector formalism to determine circular polarization purity where

$$\text{Degree of Circular Polarization} = \frac{\sqrt{|1-a^2-b^2|}}{1+\sqrt{a^2+b^2}} \quad (1)$$

where $a = (I_{(0)} - I_{(90)})/(I_{(0)} + I_{(90)})$ and $b = (I_{(45)} - I_{(315)})/(I_{(0)} + I_{(90)})$ and values in subscripts correspond to the angle of rotation in degrees. When correctly calibrated, the addition of the compensator allowed for near-perfect circular polarization (>97%) for sequential SHG-CD measurements at 890, 830, and 780 nm excitations analyzing the same field of view. By setting this threshold for calibration tolerance, we were able to standardize our instrument for consistent analysis.

We can also visualize the degree of circularity by SHG imaging of objects with cylindrical symmetry. Here, the LHCP and RHCP state at the focus was verified by SHG imaging of GUVs stained with Di-8-ANEPPS imaged at each excitation wavelength.[34] Representative images with corresponding top-and side-view 3D surface plots of both acceptable and unacceptable circular polarization examples are shown in Figure 1. If the polarization is correctly calibrated and excitation is near-perfectly circular, the emission profile will appear radially uniform, as shown in Figure 1a and b. Unacceptable calibration will result in nonuniform pixel intensities around the GUV, where an example is depicted in Figure 1c, where the higher intensity regions at ~5 and 11 o'clock delineated by black arrows (both side and top views) are indicative of linear polarization contamination.

2.4. Acquisition and Analysis of Images

SHG-CD images were acquired for tendon and collagen gel models at 780, 830, and 890 nm excitation wavelengths. We previously characterized the SHG intensity across this wavelength range.[35] Mouse-tail tendon is well characterized, and we use this to benchmark the SHG-CD response as the different wavelengths. However, this tissue is highly scattering, where this will distort the excitation polarization even within the 100 μm thickness. To reduce this effect, the tendon was first optically cleared by immersing in 50% glycerol, where we have shown this treatment preserves polarization signatures.[19] Tendon and three experimental collagen gel replicates of each concentration mixture were imaged with LHCP and RHCP excitations at 10 separate locations using three excitation wavelengths in succession, so the same field of view could be directly compared. The normalized SHG intensity data represents the average of all LHCP and RHCP images from one gel set and is normalized to maximum values of the summed SHG intensity for both, where the values represent averages from a whole image.

Images were obtained midway through the thickness of the tendon and 30 μm deep into the ~100 μm thick gel samples to be deep enough to avoid boundary effects. Gels of this concentration and cleared tendon have scattering lengths much longer than their physical thickness; thus, the measurements are not compromised by scattering. To account for variations in intensity in the different collagen mixtures, we report the normalized SHG-CD response as defined by

$$I_{\text{SHG- CD}} = \frac{|I_{(2\omega)\text{LHCP}} - I_{(2\omega)\text{RHCP}}|}{(I_{(2\omega)\text{LHCP}} + I_{(2\omega)\text{RHCP}})/2} \quad (2)$$

where $I_{(2\omega)\text{LHCP}}$ and $I_{(2\omega)\text{RHCP}}$ represent the integrated pixel intensities of the SHG images for LHCP and RHCP, respectively. This is calculated on a pixel basis, where we set a threshold above the background and made a binary mask. The pixel values of $I_{\text{SHG-CD}}$ were then summed across the entire field of view to obtain the normalized SHG-CD response.

As a control to eliminate the possibility of birefringence artifacts in the SHG-CD response, birefringence values for the 100% Col I gel and optically cleared tendon were determined at 780 nm. We performed this using linear-polarized light rotated over 0–180° in 10° increments into the stationary sample while measuring the transmitted light intensity with an analyzing Glan-Laser polarizer crossed at 90° relative to each linear input polarization. This is equivalent to fixing crossed polarizers and rotating the specimen and is performed in this way, as it is more accurate on our system. We next calculated birefringence values by $I_1 = I_0 \sin^2 2\gamma \sin^2 \frac{\delta}{2}$, where γ and δ are the azimuth and the phase difference of the sample, respectively, and I_0 and I_1 are the intensities of the light going into the sample and exiting the analyzer, respectively. We solved for δ every 10 degrees of rotation and then used the equation $\delta = \frac{2\pi \Delta n L}{\lambda}$ to solve for Δn and then used the maximum value for the calculation. Correlation of the resulting birefringence and corresponding SHG images of the gel and cleared tendon was also performed using several different correlation methods (Pearson's, Spearman's, or Kendall Tau-B).

2.5. Statistical Analyses

All of the statistical analyses were performed using SAS software (SAS institute, Cary, NC). Three experimental replicates of the gels were performed to reach the appropriate sample size. All collagen gels in each replicate were self-assembled at the same time to allow direct comparisons across all 0–40% Col III concentrations. Non-parametric Friedman's two-way ANOVA analyses, in which the individual collagen gels were ranked, were used to account for the differences in absolute values between runs. As we have previously shown, this is necessary as the degree of polymerization in collagen gels is not completely reproducible, although the results within each synthesis are directly comparable.[24] Ranks are statistically significant ($p < 0.05$) when there are no overlapping letters in the rank assignment.

3. RESULTS

3.1. SHG-CD of Tendon

Our previous report (without wavelength dependence) of SHG-CD used a different modulation approach than that used here.[27] Thus, we first measured the response at 890 nm using cleared mouse-tail tendon to verify that we found the same sensitivity. Tendon is further convenient, as the collagen is highly aligned as is expected to have as large of a response as any collagen dominant tissue. Representative SHG images of the tendon imaged with LHCP and RHCP at 890 nm are shown in Figure 2a and b, respectively. The pixel maps

of the SHG-CD response of those images are shown in Figure 2c, where positive and negative differences are shown in red and blue, respectively. However, in this case, the fibers, as well as their contained collagen molecules, are primarily aligned in the same direction and the values are essentially all unidirectional (here red). Importantly, despite differences in how excitation polarization was modulated, the SHG-CD measurements performed here on cleared tendon matched those performed previously (although the normalization was performed differently).[27] Ten such fields of view of three tendons were acquired at 780, 830, and 890 nm excitation wavelengths, and the averaged results are depicted in Figure 2d. One-way ANOVA analysis showed no statistical significance between wavelength groups ($p = 0.086$); however, two tailed student's t tests comparing 780 nm results to those obtained with 890 nm excitation showed a statistical difference ($p < 0.05$).

3.2. SHG-CD of Mixed Col I/Col III Fibrillar Gels

We next compared the SHG intensity and SHG-CD response of the series of Col I/Col III gels at the three excitation wavelengths. Representative images of the RHCP, LHCP, and SHG-CD at 780 nm excitation over the range 0–40% Col III are shown in Figure 3. In general, these gels appeared similar to what was seen previously by Tilbury et al.[24] Specifically, the SHG images are comprised of shorter and more sparsely arranged collagen fibers as the percentage of Col III concentration increased, where 0–15% gels appear relatively similar in overall morphology while exhibiting quantitatively distinct intensities (see below). Higher concentrations of Col III result in shorter and more random collagen fibers/fibrils and eventually become pixelated, presumably due to a decrease in organization from comingling of the two isoforms.

This is further validated when analyzing measurements of normalized SHG intensity of the images shown in Figure 4. First, we observed a decrease in intensity with increasing Col III, presumably due to decreasing organization, where the overall concentration is constant. We also found an increase in intensity at shorter excitation wavelengths. The latter is consistent with our previous wavelength-dependent results on tendon and on ovarian tumors, suggesting collagen tissues (and models thereof) display similar SHG properties.[35]

The normalized SHG-CD determinations (eq 2) for all the gel experiments averaged together at the three excitation wavelengths are displayed in Figure 5. We make two preliminary observations. First, we observe a different sign of the SHG-CD response for differently oriented fibrils (Figure 3). This is because the collagen molecules have an overall right handedness, and it has been shown by Barzda and co-workers that the collagen molecules lie at a near 0 angle relative to the axis of the fibril.[36] As a result, the fibril has an overall handedness, along the length, as all the collagen molecules align in the same direction, e.g., having the same C–N terminus or N–C terminus orientation all the way throughout. The result will then be an overall right or left handedness depending on the N–C or C–N direction as the fibril was made. For example, the chirality in the tendon image over a small field of view is essentially all in the same direction, as the fibers are aligned very predominantly in one direction. To further validate this, we rotated an optically cleared tendon on the microscope stage by 180° and observed the change in SHG-CD sign for the same fibrils/fibers within the fascicle (data not shown). Moreover, the fibrils within the

higher concentration Col III gels (20 and 40%) display a more random distribution of SHG-CD sign than the lower counterparts with more discrete fibrils of clear orientation. This is also consistent with the significantly decreased SHG intensity at higher Col III concentrations (Figure 4). We note that, while fibrils parallel to the laser propagation may be expected to have the largest chiral response, these are SHG inactive via the electric dipole interaction due to the near 0° molecular alignment within the fiber. Thus, there will be a distribution of tilt angles that can be observed in any given optical section of the gel. We stress that the tilt angle out of plane cannot be determined within 2D single optical sections and the SHG visualized is the orientation within the 2D plane.

Overall, the data in Figure 5 show a clear increase in SHG-CD, and thus net chirality, at shorter excitation wavelengths. This is likely because the shorter excitation wavelengths are closer in proximity to the nearest 2-photon absorption band (see the Discussion). We further note that the response decreases with increasing Col III content, most likely due to the differences in helix angle in the Col I and Col III and thus randomization when comingling in the same fibrils. Ranks analyses across the three gel replicates were used separately across each excitation wavelength (Table 1) and Col III concentration (Table 2).

To quantify these differences, we first performed a comparison of the different mixtures at the same excitation wavelength. Examining the excitation wavelength ranks in Table 1, using the Friedman's two-way analysis test with 830 and 890 nm excitations, we were able to statistically ($p < 0.05$) differentiate 0 and 5% Col III from 10, 15, 20, and 40% Col III. For all wavelengths, although only low statistical delineation was found between intermediate concentrations (5 and 10%; 10 and 15%; 15 and 20%), we were able to distinguish 5% from 15, 20, and 40% Col III; 10% from 20 and 40% Col III; and 15% from 40% Col III. While the ranks overlapped with some of the sample groups, there is a clear trend in decreased chirality at higher Col III concentrations. It is possible that the marginal differences in structure become smaller between higher concentrations of Col III.

Next, all individual concentration data were compared against the changing excitation wavelengths via the same Friedman's two-way analysis test (Table 2). We found that the 780 nm excitation data for 0, 5, 10, and 15% concentrations were significantly different than most of their counterparts at 830 and 890 nm excitations. It must be noted that no excitation wavelengths were significantly different between Col III concentrations of 20 and 40%. Still, inspection of the ranks in Table 1 and Table 2 shows a clear decrease in net chirality with increasing wavelength and Col III concentration, although less wavelength differences were observed at larger concentrations of Col III. Thus, this analysis indicates that Col III concentration rather than excitation wavelength was the most contributing factor to changes in the measured differences.

We stress that the fibrillar gels are not as reproducible of a system as an organic thin film. The absolute degree of polymerization is well-known to be highly sensitive to seemingly small differences in factors such as temperature, duration, time out of the incubator, etc. Thus, the polymerization is not a reproducible effect; however, trends within a given set can be compared.[37] We further note that, when using a linear polarization analysis that extracts the helix pitch angle, some of the neighboring Col III concentrations were also not

distinguishable. However, the 0 and 5% Col III were different from higher concentrations, consistent with the SHG-CD data supporting a large structural change occurs with even low Col III content.[24] This could be the most physiologically relevant comparison, as smaller changes in composition would most likely be expected in early stage disease, which is the most critical.

4. DISCUSSION

As this is the first wavelength-dependent SHG-CD paper on fibrillar collagen tissues, we needed to verify that the response was not due to potential confounding factors such as birefringence and tissue anisotropy. Using a transmission geometry of the 780 nm excitation wavelength and analyzing the light through crossed polarizers every 10° through 180° of rotation, we found minimal rotation due to the presence of the gel, where the correlation coefficients between the birefringence and SHG-CD images were ~0.02. Moreover, the birefringence was ~0.00091. Given the approximate midpoint of the imaging location in the gel, this corresponded to an insignificant ~25 nm (1/30 wavelength) phase retardance.

We further measured this response on the mouse-tail tendon, for both the uncleared (native) and optically cleared specimens. Here we found strong birefringence for the former, which is expected as we previously showed significant depolarization in the same tissue[38] and is consistent with the results of Schanne-Klein and co-workers on tendon.[39] The cleared tendon showed lower but still measurable birefringence (0.0025 and ~100 nm phase retardance) but still much shorter than one wavelength. The coefficient correlation between the birefringence and SHG images was somewhat higher than the gels (~0.35). Still, we note that the SHG-CD wavelength dependences of the tendon and 100% Col I gels were similar, although the latter was slightly lower in magnitude. This is likely due to overlapping fibrils within the focal volume with opposite SHG-CD signs, where this results in a reduced net response. Lastly, there were no correlated rotational or orientational effects on the SHG-CD response from the gels or cleared tendon, which showed that anisotropy is not coupled into the measured values.[40] Specifically, we analyzed the SHG-CD response from randomly oriented fibrils within a 100% Col I gel by rotating the gel from 0 to 360° in 10° increments and found the response had a standard deviation of only ~2% of the average (0.48 ± 0.009), with no correlation with orientation. Analogously, analysis of the same 0–360° rotational SHG-CD response of tendon showed only a slightly higher standard deviation of ~3% (0.216 ± 0.007), where these deviations are comparable to the intrinsic error of the measurement. We note that there may be an axial dependence; however, our experimental setup is not sensitive to that dimensional dependence.

As a further validation, we previously used SHG-CD at one wavelength (890 nm) to compare the response from normal human skin tissues with those from patients with the connective tissue disorder osteogenesis imperfecta.[27] In the latter, the collagen is misfolded, and we postulated that there may be a different SHG response due to the change in chirality. This was indeed the case, where the misfolded collagen produced a 2-fold lower SHG-CD response. We note that, by simple inspection, the images were not strikingly different; thus, the only significant difference was the secondary and tertiary structure of the collagen.

Collectively, these observations show that the wavelength-dependent SHG-CD response is a valid means to probe changes in collagen chirality.

One goal of this work was to begin to understand the mechanism of SHG-CD in collagen tissues, as it may provide a new tool for imaging changes in diseased states. This need remains, as the bulk of prior SHG-CD work has examined this process on thin films. Two distinct mechanisms have been proposed, on the basis of either local electric-dipole (μ_e) or nonlocal magnetic-dipole (μ_m) transitions.[22,29,41] The former, or Kuhn model, is based on coupled local oscillators, and because this is a purely electric interaction, a significant wavelength dependence in the SHG-CD response would be expected. The nonlocal magnetic, or Kauzmann, model describes the interaction of an electron with a helix and has been proposed to explain chirality in assembled helical polymers such as helicenes in thin films. Relatedly, in their sum frequency generation studies of collagen fibrils, Knoesen et al. argued that higher ordered structures were the source of the observed nonlinear chirality.[42] In contrast, Simpson showed the electric dipole mechanism was dominant in thin films of bacteriorhodopsin, with minimal magnetic dipole contributions.[41]

To explore these possibilities on the origin of chirality in the SHG response, we measured the SHG-CD at three different wavelengths. In both tendon and collagen gels, we observed approximately a significant increase in the SHG-CD response between 890 and 780 nm excitation. This is suggestive of a strong role of the coupled oscillator model, where the shorter wavelength is nearer in energy to an electronic resonance. In general, the wavelength dependence of SHG efficiency can be expressed as the two-state model[43]

$$d_{\text{eff}}{}^2 \propto \beta^2 = \left(\frac{3e^2}{2m\hbar} \frac{\omega_0 f \Delta\mu}{(\omega_0{}^2 - \omega_1{}^2)(\omega_0{}^2 - \omega_2{}^2)} \right)^2 \quad (3)$$

where ω_0 is the resonance frequency of an absorption band and ω_1 and ω_2 are the excitation and emission angular frequencies, respectively; f and $\Delta\mu$ represent oscillator strength and change in dipole moments between ground and excited states, respectively. As the energies of either the excitation and/or SHG emission frequencies approach either a one- or two-photon absorption band, the intensity of SHG will be resonance enhanced. If the Kuhn model is applicable, then the SHG-CD should also be increased at the shorter excitation wavelengths, and this is indeed observed here. By contrast, the magnetic interaction based on higher order structures would not be expected to have a strong wavelength dependence. While our results are consistent with the Kuhn model, it may not be possible to directly isolate the magnetic contribution.[29] As fibrillar collagen is comprised of higher ordered structures, we conclude that both mechanisms are likely operative in these tissues. However, we can rule out the role of anisotropy due to fibril orientation, which can be erroneously coupled into the observed chiral response.[40]

The wavelength dependence of the SHG intensity has been discussed in previous reports.[44–47] Rigorously taking into account experimental factors and optical scattering, we showed a strong wavelength dependence, where the maximum response was observed at the

780 nm excitation, the shortest wavelength used.[35] The nature of the nearest possible resonance in collagen remains unclear, but we note that we have previously shown that Kleinman's symmetry is not valid in this wavelength range.[21] While it may not be directly connected to SHG, the nearest collagen absorption corresponds to that of cross-linked collagen, peaking at ~360 nm (or 720 nm for two-photon absorption).[48] We previously fit our wavelength-dependent measurements of tendon to the two-level model (eq 3) using this transition, and although the overall trend was similar, we did not find an accurate fit.[35] In contrast, the 190–220 nm absorption bands in molecular collagen (and those used in linear CD) showed much larger deviations in the fit.

Overall, our data suggests the wavelength dependence of the SHG-CD response follows that of the wavelength-dependent SHG conversion efficiency.[35] It is thus likely that the SHG-CD would further increase at shorter wavelengths. However, this would result in a sharp decrease in emission detection due to decreased transmission in glass at wavelengths < ~380 nm. Furthermore, while scattering is negligible for these fibrillar gels ($\mu_s \sim 6\ cm^{-1}$), scattering coefficients in intact collagenous tissues are much higher (~200–500 cm^{-1}), and the excitation will be more susceptible to polarization scrambling at shorter wavelengths. Given the decreased sensitivity in the SHG-CD at 890 nm, it does not appear beneficial to perform these measurements at longer wavelengths.

The use of SHG-CD adds to the repertoire of polarization-resolved SHG metrics for examining collagen attributes on nano/microscales. We recently implemented a pixel-based approach combining the single-axis model[21,49] and the more recent generic model[23] to extract α-helical pitch angles within collagen molecules as well as SHG signal anisotropy for probing dipolar order.[24] We used this approach to characterize the analogous gels comprised of Col I and III mixtures,[24] and the results from this study were consistent with previous optical-based experiments as well as structural biology litera-ture.[21,42,49–52] The decrease in net chirality with increasing Col III observed here compliments the pixel-based approaches, which showed a net change in pitch angle and dipole alignment, as it provides a different, but related, output. Lastly, the method only requires two images per optical section, whereas the full pixel-based linear polarization requires either 19 or 381 (with polarization analysis).[24] This short acquisition time lends itself to future translational applications.

We note that much can be gained for understanding structural changes in diseases such as cancers and fibroses even with model tissues and thin ex vivo slices as used here. For example, in our work on human ovarian tissues, we imaged 100 μm thick slices, and this provides substantial information as, in ovary, the major changes occur at this depth.[13] This would also apply to either ex vivo or in vivo skin. We believe such studies using model tissues and ex vivo slices are critical for any future diagnostic purposes (either ex vivo or in vivo). They can also provide insight that is valuable for understanding disease etiology and may identify future therapeutic targets. The SHG-CD contrast provides another metric to the tissue characterization. Moreover, there are no moving parts in the polarization modulation, and the technique could be implemented in a small, stable footprint. While the data acquisition for this study utilizes forward emission detection, a backward SHG detection geometry could also be used, albeit with lower signal magnitude.

A potential limitation of linear SHG polarization methods in general is that, due to birefringence, the polarization (either of the excitation laser or SHG signal) will become scrambled within two to three scattering lengths.[53] However, there are suggestions that circularly polarized light is less sensitive to depolarization than linear polarization.[54,55] Still, we observed that the birefringence in native tendon was significant, but this was greatly reduced in optically cleared tendon. Optical clearing agents, which essentially eliminate scattering and retain polarization signatures, are routinely used on ex vivo tissues and have shown promise for in vivo applications.[53,56] The SHG-CD technique could analyze a wide range of pathologies known to exhibit a change in collagen assembly at the molecular scale, including wound healing, connective tissue disorders, idiopathic pulmonary fibrosis, scleroderma, corneal disease, and other epithelial cancers.

5. CONCLUSIONS

Our most important goal in the work was to further develop SHG-CD imaging on a laser scanning microscope to probe differences in chirality in model tissues of ovarian cancer. The geometry is different than that used for SHG-CD of thin films, and optimizing the instrumentation, especially the careful use of compensation, was essential to perform this at different wavelengths and optimizing sensitivity and accuracy of the response. Using this method, we found that collagen gels of differing Col I and III composition serving as ovarian cancer stromal models have quantifiable changes in net chirality due to different helical properties in each isoform. The increase in SHG-CD response at shorter wavelengths, nearer to a collagen absorption band, is consistent with the Kuhn coupled oscillator model proposed for the nonlinear chirality on thin films. We believe this technique would be useful for making comparative quantifications of many normal versus diseased tissues. Furthermore, the accurate and precise polarization modulation without motion artifacts makes this approach attractive for use in a laparoscope or endoscope.

Acknowledgments

Funding for this work was supported by the National Science Foundation (NSF) CBET-1402757 (P.J.C.) and the National Cancer Institute of the National Institutes of Health under Award Numbers T32CA009206 (K.R.C.). The content is solely the responsibility of the authors and does not necessarily represent the official views of the National Institutes of Health. We gratefully acknowledge the contributions of Dr. Karissa Tilbury of University of Maine-Orono for technical help and Dr. Peter Crump of the University of Wisconsin-Madison for statistical assistance.

References

1. Ricciardelli C, Rodgers RJ. Extracellular Matrix of Ovarian Tumors. Semin Reprod Med. 2006; 24:270–82. [PubMed: 16944424]
2. Nelson AR, Fingleton B, Rothenberg ML, Matrisian LM. Matrix Metalloproteinases: Biologic Activity and Clinical Implications. J Clin Oncol. 2000; 18:1135–49. [PubMed: 10694567]
3. Pupa SM, Menard S, Forti S, Tagliabue E. New Insights into the Role of Extracellular Matrix During Tumor Onset and Progression. J Cell Physiol. 2002; 192:259–267. [PubMed: 12124771]
4. Kauppila S, Bode MK, Stenback F, Risteli L, Risteli J. Cross-Linked Telopeptides of Type I and Iii Collagens in Malignant Ovarian Tumours in Vivo. Br J Cancer. 1999; 81:654–61. [PubMed: 10574251]

5. Sherman-Baust CA, Weeraratna AT, Rangel LB, Pizer ES, Cho KR, Schwartz DR, Shock T, Morin PJ. Remodeling of the Extracellular Matrix through Overexpression of Collagen Vi Contributes to Cisplatin Resistance in Ovarian Cancer Cells. Cancer Cell. 2003; 3:377–86. [PubMed: 12726863]
6. Brown E, McKee T, diTomaso E, Pluen A, Seed B, Boucher Y, Jain RK. Dynamic Imaging of Collagen and Its Modulation in Tumors in Vivo Using Second-Harmonic Generation. Nat Med. 2003; 9:796–800. [PubMed: 12754503]
7. Provenzano PP, Eliceiri KW, Campbell JM, Inman DR, White JG, Keely PJ. Collagen Reorganization at the Tumor-Stromal Interface Facilitates Local Invasion. BMC Med. 2006; 4:38. [PubMed: 17190588]
8. Cicchi R, Massi D, Sestini S, Carli P, De Giorgi V, Lotti T, Pavone FS. Multidimensional Non-Linear Laser Imaging of Basal Cell Carcinoma. Opt Express. 2007; 15:10135–48. [PubMed: 19547362]
9. Le TT, Langohr IM, Locker MJ, Sturek M, Cheng JX. Label-Free Molecular Imaging of Atherosclerotic Lesions Using Multimodal Nonlinear Optical Microscopy. J Biomed Opt. 2007; 12:054007. [PubMed: 17994895]
10. Strupler M, Pena AM, Hernest M, Tharaux PL, Martin JL, Beaurepaire E, Schanne-Klein MC. Second Harmonic Imaging and Scoring of Collagen in Fibrotic Tissues. Opt Express. 2007; 15:4054–65. [PubMed: 19532649]
11. Kwon GP, Schroeder JL, Amar MJ, Remaley AT, Balaban RS. Contribution of Macromolecular Structure to the Retention of Low-Density Lipoprotein at Arterial Branch Points. Circulation. 2008; 117:2919–27. [PubMed: 18506002]
12. Sun W, Chang S, Tai DC, Tan N, Xiao G, Tang H, Yu H. Nonlinear Optical Microscopy: Use of Second Harmonic Generation and Two-Photon Microscopy for Automated Quantitative Liver Fibrosis Studies. J Biomed Opt. 2008; 13:064010. [PubMed: 19123657]
13. Nadiarnykh O, Lacomb RB, Brewer MA, Campagnola PJ. Alterations of the Extracellular Matrix in Ovarian Cancer Studied by Second Harmonic Generation Imaging Microscopy. BMC Cancer. 2010; 10:94. [PubMed: 20222963]
14. Chaudhary R, Campbell KR, Tilbury KB, Vanderby R Jr, Block WF, Kijowski R, Campagnola PJ. Articular Cartilage Zonal Differentiation Via 3d Second-Harmonic Generation Imaging Microscopy. Connect Tissue Res. 2015; 56:76–86. [PubMed: 25738523]
15. Suhalim JL, Chung CY, Lilledahl MB, Lim RS, Levi M, Tromberg BJ, Potma EO. Characterization of Cholesterol Crystals in Atherosclerotic Plaques Using Stimulated Raman Scattering and Second-Harmonic Generation Microscopy. Biophys J. 2012; 102:1988–95. [PubMed: 22768956]
16. Pena AM, Fabre A, Debarre D, Marchal-Somme J, Crestani B, Martin JL, Beaurepaire E, Schanne-Klein MC. Three-Dimensional Investigation and Scoring of Extracellular Matrix Remodeling During Lung Fibrosis Using Multiphoton Microscopy. Microsc Res Tech. 2007; 70:162–70. [PubMed: 17177275]
17. Campagnola PJ, Loew LM. Second-Harmonic Imaging Microscopy for Visualizing Biomolecular Arrays in Cells, Tissues and Organisms. Nat Biotechnol. 2003; 21:1356–60. [PubMed: 14595363]
18. Nadiarnykh O, Plotnikov S, Mohler WA, Kalajzic I, Redford-Badwal D, Campagnola PJ. Second Harmonic Generation Imaging Microscopy Studies of Osteogenesis Imperfecta. J Biomed Opt. 2007; 12:051805. [PubMed: 17994883]
19. LaComb R, Nadiarnykh O, Carey S, Campagnola PJ. Quantitative Second Harmonic Generation Imaging and Modeling of the Optical Clearing Mechanism in Striated Muscle and Tendon. J Biomed Opt. 2008; 13:021109. [PubMed: 18465958]
20. Lee WJ, Lee CF, Chen SY, Chen YS, Sun CK. Virtual Biopsy of Rat Tympanic Membrane Using Higher Harmonic Generation Microscopy. J Biomed Opt. 2010; 15:046012. [PubMed: 20799814]
21. Plotnikov SV, Millard AC, Campagnola PJ, Mohler WA. Characterization of the Myosin-Based Source for Second-Harmonic Generation from Muscle Sarcomeres. Biophys J. 2006; 90:693–703. [PubMed: 16258040]
22. Tuer AE, Krouglov S, Prent N, Cisek R, Sandkuijl D, Yasufuku K, Wilson BC, Barzda V. Nonlinear Optical Properties of Type I Collagen Fibers Studied by Polarization Dependent Second Harmonic Generation Microscopy. J Phys Chem B. 2011; 115:12759–69. [PubMed: 21970315]

23. Duboisset J, Äit-Belkacem D, Roche M, Rigneault H, Brasselet S. Generic Model of the Molecular Orientational Distribution Probed by Polarization-Resolved Second-Harmonic Generation. Phys Rev A: At, Mol, Opt Phys. 2012; 85:27.
24. Tilbury K, Lien CH, Chen SJ, Campagnola PJ. Differentiation of Col I and Col Iii Isoforms in Stromal Models of Ovarian Cancer by Analysis of Second Harmonic Generation Polarization and Emission Directionality. Biophys J. 2014; 106:354–65. [PubMed: 24461010]
25. Hicks JM, Petralli-Mallow T. Nonlinear Optics of Chiral Surface Systems. Appl Phys B: Lasers Opt. 1999; 68:589–593.
26. Botek E, Andre JM, Champagne B, Verbiest T, Persoons A. Mixed Electric-Magnetic Second-Order Nonlinear Optical Response of Helicenes. J Chem Phys. 2005; 122:234713. [PubMed: 16008479]
27. Chen XY, Raggio C, Campagnola PJ. Second-Harmonic Generation Circular Dichroism Studies of Osteogenesis Imperfecta. Opt Lett. 2012; 37:3837–3839. [PubMed: 23041876]
28. Lee H, Huttunen MJ, Hsu KJ, Partanen M, Zhuo GY, Kauranen M, Chu SW. Chiral Imaging of Collagen by Second-Harmonic Generation Circular Dichroism. Biomed Opt Express. 2013; 4:909–16. [PubMed: 23761852]
29. Hache F, Mesnil H, Schanne-Klein MC. Application of Classical Models of Chirality to Surface Second Harmonic Generation. J Chem Phys. 2001; 115:6707–6715.
30. Barsky SH, Rao CN, Grotendorst GR, Liotta LA. Increased Content of Type V Collagen in Desmoplasia of Human Breast Carcinoma. Am J Pathol. 1982; 108:276–83. [PubMed: 6287844]
31. Seyer JM, Hutcheson ET, Kang AH. Collagen Polymorphism in Idiopathic Chronic Pulmonary Fibrosis. J Clin Invest. 1976; 57:1498–507. [PubMed: 777026]
32. Keely PJ, Fong AM, Zutter MM, Santoro SA. Alteration of Collagen-Dependent Adhesion, Motility, and Morphogenesis by the Expression of Antisense Alpha 2 Integrin Mrna in Mammary Cells. J Cell Sci. 1995; 108(Pt 2):595–607. [PubMed: 7769004]
33. Sandre O, Moreaux L, Brochard-Wyart F. Dynamics of Transient Pores in Stretched Vesicles. Proc Natl Acad Sci U S A. 1999; 96:10591–10596. [PubMed: 10485870]
34. Lien CH, Tilbury K, Chen SJ, Campagnola PJ. Precise, Motion-Free Polarization Control in Second Harmonic Generation Microscopy Using a Liquid Crystal Modulator in the Infinity Space. Biomed Opt Express. 2013; 4:1991–2002. [PubMed: 24156059]
35. Hall G, Tilbury KB, Campbell KR, Eliceiri KW, Campagnola PJ. Experimental and Simulation Study of the Wavelength Dependent Second Harmonic Generation of Collagen in Scattering Tissues. Opt Lett. 2014; 39:1897–1900. [PubMed: 24686633]
36. Tuer AE, Akens MK, Krouglov S, Sandkuijl D, Wilson BC, Whyne CM, Barzda V. Hierarchical Model of Fibrillar Collagen Organization for Interpreting the Second-Order Susceptibility Tensors in Biological Tissue. Biophys J. 2012; 103:2093–105. [PubMed: 23200043]
37. Raub CB, Suresh V, Krasieva T, Lyubovitsky J, Mih JD, Putnam AJ, Tromberg BJ, George SC. Noninvasive Assessment of Collagen Gel Microstructure and Mechanics Using Multiphoton Microscopy. Biophys J. 2007; 92:2212–22. [PubMed: 17172303]
38. Nadiarnykh O, Campagnola PJ. Retention of Polarization Signatures in Shg Microscopy of Scattering Tissues through Optical Clearing. Opt Express. 2009; 17:5794–5806. [PubMed: 19333348]
39. Gusachenko I, Latour G, Schanne-Klein MC. Polarization-Resolved Second Harmonic Microscopy in Anisotropic Thick Tissues. Opt Express. 2010; 18:19339–19352. [PubMed: 20940829]
40. Sioncke S, Van Elshocht S, Verbiest T, Persoons A, Kauranen M, Phillips KES, Katz TJ. Optical Activity Effects in Second Harmonic Generation from Anisotropic Chiral Thin Films. J Chem Phys. 2000; 113:7578–7581.
41. Wampler RD, Zhou M, Thompson DH, Simpson GJ. Mechanism of the Chiral Shg Activity of Bacteriorhodopsin Films. J Am Chem Soc. 2006; 128:10994–10995. [PubMed: 16925395]
42. Rocha-Mendoza I, Yankelevich DR, Wang M, Reiser KM, Frank CW, Knoesen A. Sum Frequency Vibrational Spectroscopy: The Molecular Origins of the Optical Second-Order Nonlinearity of Collagen. Biophys J. 2007; 93:4433–44. [PubMed: 17766339]
43. Oudar JL, Chemla DS. Hyperpolarizabilities of the Nitroanilines and Their Relations to the Excited State Dipole Moment. J Chem Phys. 1977; 66:2664–2668.

44. Zoumi A, Yeh A, Tromberg BJ. Imaging Cells and Extracellular Matrix in Vivo by Using Second-Harmonic Generation and Two-Photon Excited Fluorescence. Proc Natl Acad Sci U S A. 2002; 99:11014–9. [PubMed: 12177437]
45. Zipfel WR, Williams RM, Webb WW. Nonlinear Magic: Multiphoton Microscopy in the Biosciences. Nat Biotechnol. 2003; 21:1369–77. [PubMed: 14595365]
46. Theodossiou TA, Thrasivoulou C, Ekwobi C, Becker DL. Second Harmonic Generation Confocal Microscopy of Collagen Type I from Rat Tendon Cryosections. Biophys J. 2006; 91:4665–77. [PubMed: 17130233]
47. Shen M, Zhao J, Zeng H, Tang S. Calibrating the Measurement of Wavelength-Dependent Second Harmonic Generation from Biological Tissues with a Bab(2)O(4) Crystal. J Biomed Opt. 2013; 18:031109. [PubMed: 23396547]
48. Richards-Kortum R, Sevick-Muraca E. Quantitative Optical Spectroscopy for Tissue Diagnosis. Annu Rev Phys Chem. 1996; 47:555–606. [PubMed: 8930102]
49. Su PJ, Chen WL, Chen YF, Dong CY. Determination of Collagen Nanostructure from Second-Order Susceptibility Tensor Analysis. Biophys J. 2011; 100:2053–62. [PubMed: 21504742]
50. Beck K, Brodsky B. Supercoiled Protein Motifs: The Collagen Triple-Helix and the Alpha-Helical Coiled Coil. J Struct Biol. 1998; 122:17–29. [PubMed: 9724603]
51. Tiaho F, Recher G, Rouede D. Estimation of Helical Angles of Myosin and Collagen by Second Harmonic Generation Imaging Microscopy. Opt Express. 2007; 15:12286–95. [PubMed: 19547597]
52. Nucciotti V, Stringari C, Sacconi L, Vanzi F, Fusi L, Linari M, Piazzesi G, Lombardi V, Pavone FS. Probing Myosin Structural Conformation in Vivo by Second-Harmonic Generation Microscopy. Proc Natl Acad Sci U S A. 2010; 107:7763–8. [PubMed: 20385845]
53. Nadiarnykh O, Campagnola PJ. Retention of Polarization Signatures in Shg Microscopy of Scattering Tissues through Optical Clearing. Opt Express. 2009; 17:5794–806. [PubMed: 19333348]
54. Ahmad M, Alali S, Kim A, Wood MF, Ikram M, Vitkin IA. Do Different Turbid Media with Matched Bulk Optical Properties Also Exhibit Similar Polarization Properties? Biomed Opt Express. 2011; 2:3248–58. [PubMed: 22162815]
55. MacKintosh FC, Zhu JX, Pine DJ, Weitz DA. Polarization Memory of Multiply Scattered Light. Phys Rev B: Condens Matter Mater Phys. 1989; 40:9342–9345.
56. Wen X, Mao Z, Han Z, Tuchin VV, Zhu D. In Vivo Skin Optical Clearing by Glycerol Solutions: Mechanism. J Biophotonics. 2010; 3:44–52. [PubMed: 19937846]

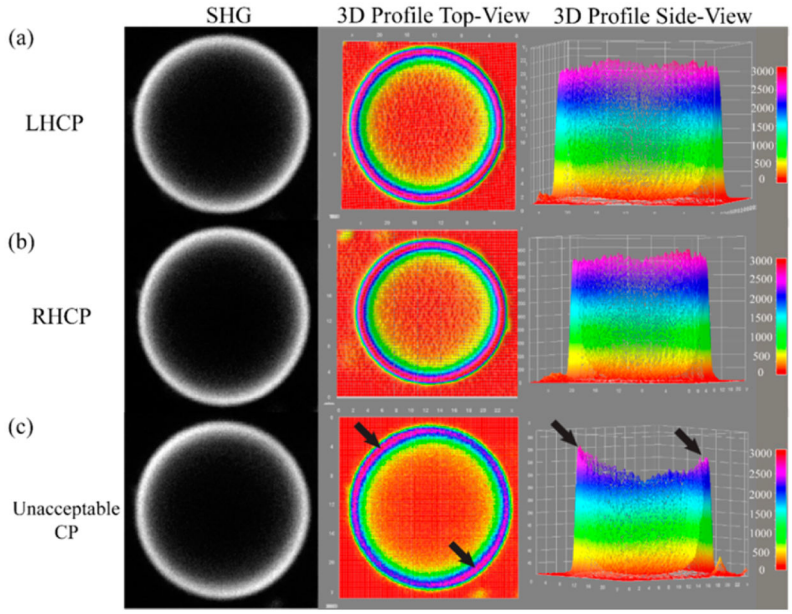

Figure 1.

Representative SHG images and corresponding 3D profiles of Di-8-ANNEPS membrane-stained giant unilamellar vesicles. Parts a and b show examples of acceptable left- and right-circular polarization. Part c is an example of unacceptable circular polarization where black arrows indicate regions of higher intensity lobes due to elliptical polarization. The field of view is 40 × 40 μm^2.

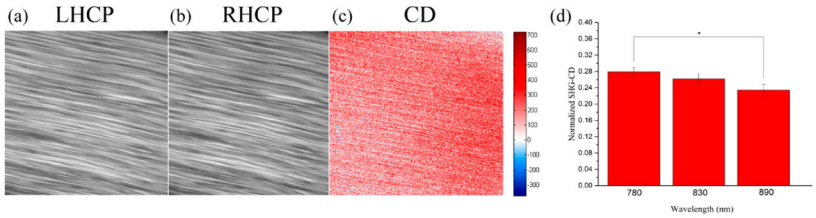

Figure 2.

Representative SHG images of mouse-tail tendon and corresponding CD response: (a) LHCP, (b) RHCP, and (c) CD. Positive and negative CD differences are given in blue and red, respectively. The field of view is 85 × 85 μm^2. Part d shows the mean normalized SHG-CD data of cleared mouse-tail tendon measured at 780, 830, and 890 nm excitation wavelengths. The asterisk denotes significance $p < 0.05$. Standard error bars are shown.

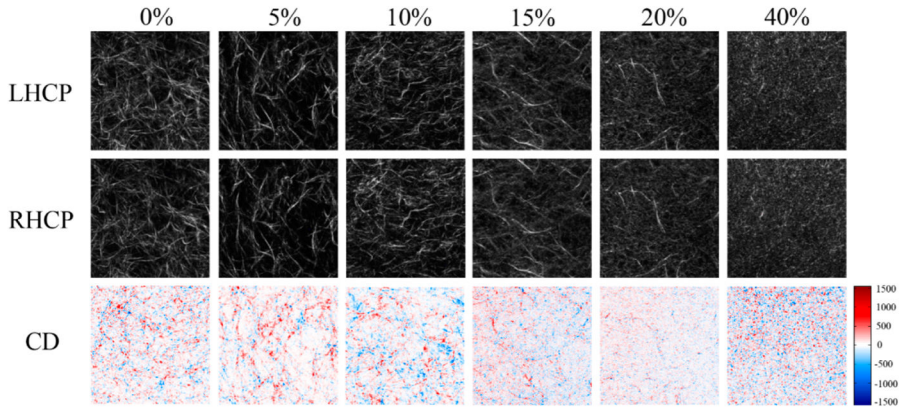

Figure 3.

Representative SHG images of increasing Col III in Col I gels for LHCP (top) and RHCP (middle) as well as the corresponding CD images (bottom). Positive and negative CD differences are given in blue and red, respectively. The field of view is 85 × 85 μm^2.

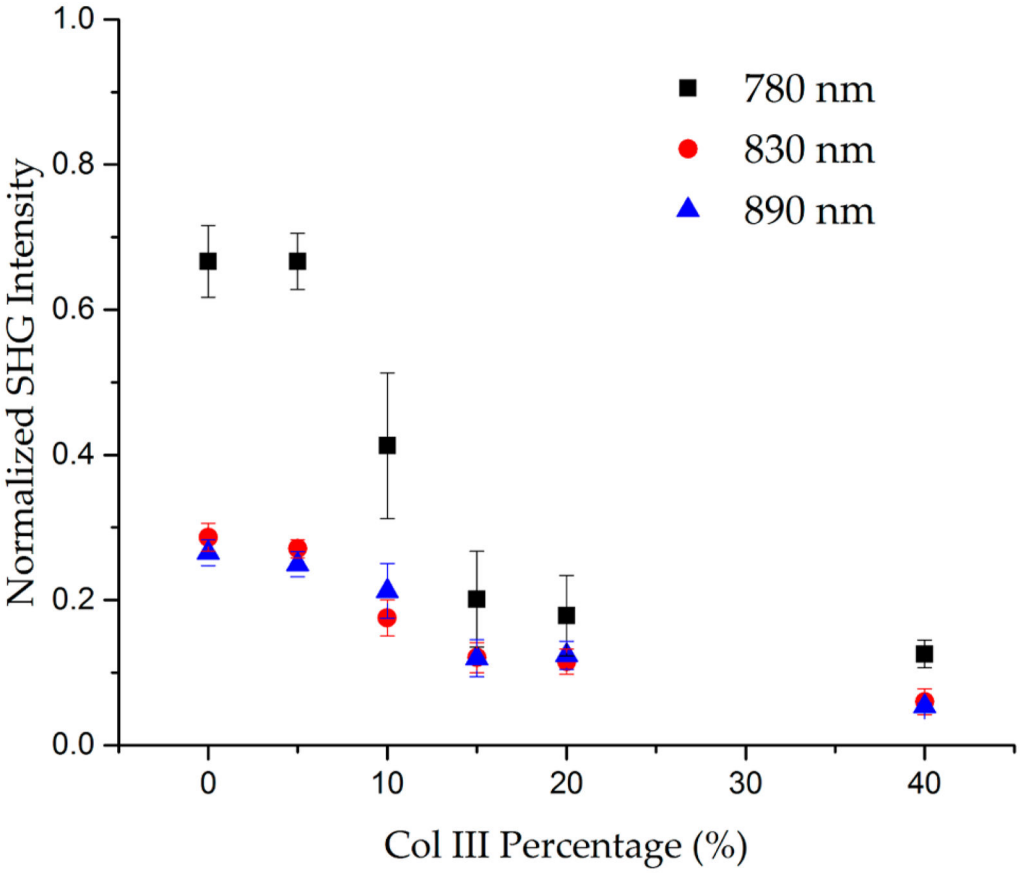

Figure 4.
Normalized SHG intensity vs increasing Col III percentage for 780, 830, and 890 nm excitations. Standard error bars are shown.

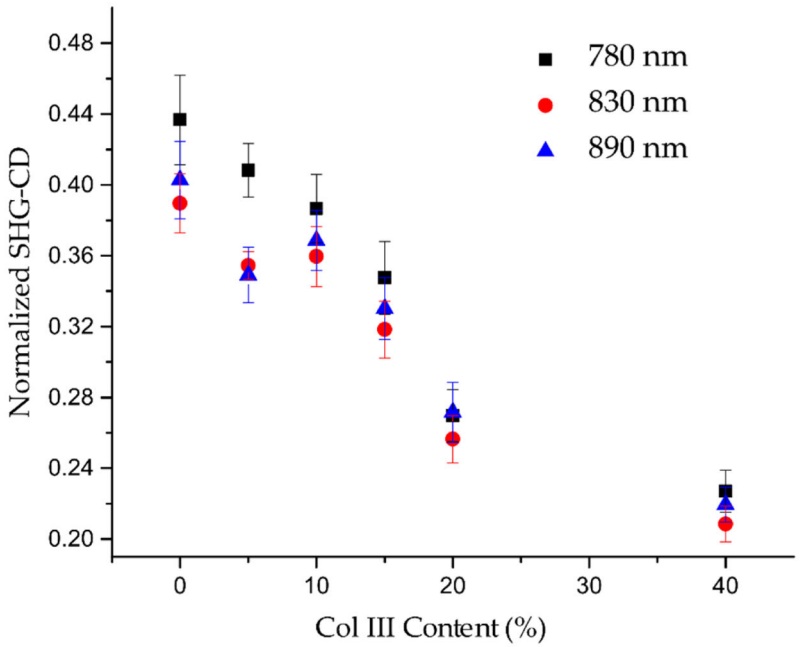

Figure 5.
Mean normalized SHG-CD vs increasing Col III percentage for all three sample sets at 780, 830, and 890 nm excitations. Standard error bars are shown.

Table 1

SHG-CD Ranks at Each Excitation Wavelength across Varying Concentrations of Col III[a]

Col III%	0%	5%	10%	15%	20%	40%
780 nm ranks	A	A	AB	BC	C	D
830 nm ranks	A	AB	B	C	C	D
890 nm ranks	A	AB	BC	CD	D	E

[a]Letter combinations of A, B, C, D, and E represent the ranks used in the nonparametric Friedman's two-way analysis, where non-overlapping letter combinations signify $p < 0.05$ significance.

Table 2

SHG-CD Ranks at Each Concentration of Col III across Varying Excitation Wavelengths[a]

Col III%	0% ranks	5% ranks	10% ranks	15% ranks	20% ranks	40% ranks
780 nm	A	A	A	A	A	A
830 nm	B	B	B	B	A	A
890 nm	AB	B	AB	B	A	A

[a]Letter combinations of A and B represent ranks used in the nonparametric Friedman's two-way analysis, where non-overlapping letter combinations signify $p < 0.05$ significance.

J Phys Chem B. Author manuscript; available in PMC 2017 July 02.